Direct molecular force measurements of multiple adhesive interactions between cadherin ectodomains

S. Sivasankar*, W. Brieher[†‡], N. Lavrik[§], B. Gumbiner[†], and D. Leckband*[§¶]

[§]Department of Chemical Engineering and *Center for Biophysics and Computational Biology, University of Illinois at Urbana–Champaign, Urbana, IL 61801; and [†]Cellular Biochemistry and Biophysics Program, Memorial Sloan–Kettering Cancer Center, New York, NY 10021

Communicated by William R. Schowalter, University of Illinois at Urbana-Champaign, Urbana, IL, August 3, 1999 (received for review March 23, 1999).

Direct-force measurements of the interactions between recombinant C-cadherin from *Xenopus* demonstrated that the ectodomain of cadherin exhibits multiple adhesive contacts that involve successive domains along the extracellular region of the protein. Contacts between the fully interdigitated antiparallel proteins form the strongest adhesive interaction. A second weaker minimum was measured when the interdigitated proteins were separated by a distance equal to the length of one domain of the extracellular (EC) fragment and corresponding to the antiparallel alignment of domains one through four (EC1 through EC4). The successive rupture of these interactions generates an unbinding force profile that may be optimized to impede the abrupt failure of cadherin-mediated junctions under force.

Cadherins constitute a class of morphoregulatory proteins that bind to identical proteins on cell surfaces to mediate cell–cell adhesion in all soft tissue (1–3). They also facilitate cell sorting during tissue morphogenesis (1–4). These are single-pass transmembrane glycoproteins, and the homophilic association of identical opposed cadherin extracellular (EC) segments maintains the intercellular interactions in adult tissues (2, 3). The latter region of classical cadherins comprises five tandemly arranged homologous domains, which are numbered from the outermost domain EC1 through EC5 (Fig. 1). This region of the complete transmembrane protein exhibits calcium-dependent homophilic binding (5, 6). The formation of lateral dimers of the extracellular segments also increases the strength of adhesive cell–cell contacts (5–7).

To date, only the crystal structures of the first segment of neural cadherin (NEC), NEC1, of the two outer domains NEC1–2 (7, 8), and of the outer two domains from epithelial cadherin (EEC1–2) (9), have been determined. Contacts between antiparallel proteins in the crystals of NEC1 suggested that homophilic adhesion involves interactions between antiparallel cis-dimers of the N-terminal domains (7, 10). The putative adhesive contacts are not, however, observed in the other crystal structures of either EEC1–2 or NEC1–2 (8, 9). This lack of antiparallel interactions between the N-terminal EC1 domains in all but one of the reported cadherin crystals brings into question the protein contacts that actually effect cell–cell binding.

To understand the molecular basis of the adhesive function of cadherin, we used direct-force measurements to quantify the interaction potential between oriented monolayers of the recombinant ectodomains of C-cadherin (11, 12). In particular, we used the surface-force apparatus to quantify both the magnitude and the distance dependence of the forces between the full-length cadherin extracellular segments. By these means, we identified three important aspects of cadherin binding. First, we determined the relative alignments of cadherin domains in the adhesive complex from the measured position that generates the maximum attractive force. Second, the measurements identified multiple adhesive contacts between the antiparallel interdigitated proteins. These sites of adhesion involve successive domains along the full extracellular segment EC1–5. The strongest interaction is between the fully interdigitated antiparallel proteins. We also identified a second weaker minimum when the interdigitated proteins were separated by a distance equal to the length of one EC domain. Finally, we show that the successive rupture of these contacts during protein detachment generates an unusual unbinding force profile, which may impede the abrupt failure of cadherin-mediated adhesive junctions under force.

Materials and Methods

Chemicals. 1,2-ditridecanoyl-*sn*-glycero-3-phosphocoline (DTPC; melting temperature T_m = 14°C) and 1,2-dipalmitoyl-*sn*-glycero-3-phosphoethanolamine (DPPE) were purchased from Avanti Polar Lipids. The copper chelating lipid distearoyl-glycerylether-iminodiacetic acid (DSIDA) was a gift from Francis Arnold (California Institute of Technology) (13). All inorganic salts were high purity (>99.5%) and were purchased from Aldrich. Tris buffer was purchased from Sigma. Slide-A-Lyzer dialysis cassettes (10,000 MW cutoff) were from Pierce. Aqueous solutions were prepared with water purified with a Milli-Q UV Plus water purification system (Millipore).

Preparation of Cadherin Monolayers. Homogeneously oriented monolayers of C-cadherin extracellular domains 1–5 (CEC1–5) with a polyhistidine tail at the C terminus (5) were immobilized on supported lipid bilayers displaying DSIDA (Fig. 1). The outer leaflet of the bilayer comprised DSIDA and DTPC at defined mol fractions. In the described measurements, cadherin was bound to membranes containing 25, 40, or 85 mol% DSIDA in a DTPC matrix. To prepare these bilayer films, a lipid mixture in a 9:1 chloroform/methanol solution was spread at the air–water interface of a Langmuir trough (NIMA, Coventry, England). After allowing the chloroform to evaporate, the monolayer was compressed to an average lipid area of 0.65 nm^2. The aqueous subphase was maintained at 25°C and contained 0.25 μM $Cu(NO_3)_2$, 50 mM Tris buffer, and 100 mM $NaNO_3$ at pH 7.5. The lipid monolayer was then transferred at constant pressure onto a monolayer of gel-phase dipalmitoyl phosphatidylethanolamine (0.43 nm^2/lipid) supported on freshly cleaved mica substrates as described previously (14, 15). Before mounting the supported bilayers in the apparatus, the disks supporting the coated mica sheets were transferred to small beakers containing 3 ml of 3 nM cadherin, 50 mM Tris buffer, 100 mM $NaNO_3$, and 1 mM $Ca(NO_3)_2$ at pH 7.5, 25°C. The protein adsorption proceeded for 1 hr, after which the buffer was exchanged for an identical solution that lacked cadherin. The

Abbreviations: EC, extracellular; NEC, neural cadherin domain; DTPC, 1,2-ditridecanoyl-*sn*-glycero-3-phosphocoline; DPPE, 1,2-dipalmitoyl-*sn*-glycero-3-phosphoethanolamine; DSIDA, distearoyl-glycerylether-iminodiacetic acid; CEC1–5, C-cadherin extracellular domains 1–5.

[‡]Present address: Department of Cell Biology, Harvard Medical School, Longwood Avenue, Boston, MA 02115.

[¶]To whom reprint requests should be addressed. E-mail: leckband@uiuc.edu.

The publication costs of this article were defrayed in part by page charge payment. This article must therefore be hereby marked "*advertisement*" in accordance with 18 U.S.C. §1734 solely to indicate this fact.

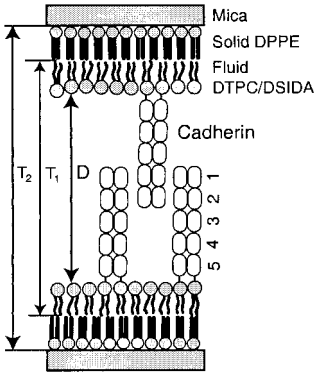

Fig. 1. Illustration of the immobilized cadherin monolayers. Recombinant cadherin CEC1–5 was immobilized on supported planar bilayers via a polyhistidine tail at the C terminus of domain 5 (5). The distal monolayer is gel phase dipalmitoyl phosphatidyl ethanolamine (0.43 nm^2/lipid) supported on atomically smooth mica sheets. The outer proximal monolayer comprises a mixture of DTPC and DSIDA in the proportions given in the text. The samples are immersed in buffer.

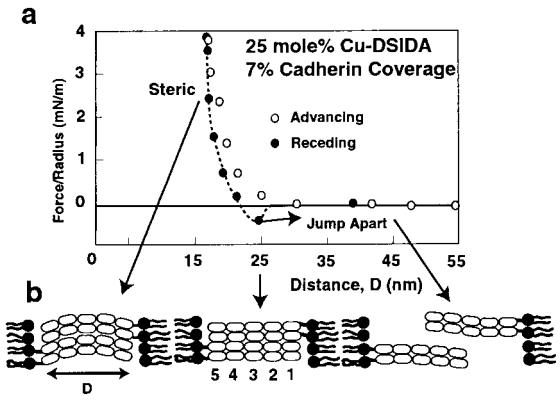

Fig. 2. (*a*) Normalized force vs. the distance *D* between immobilized cadherin ectodomains at 7% surface coverage. The interprotein force normalized by the radius of curvature *R* of the supporting discs, was measured at pH 7.5 and 25°C in 50 mM Tris buffer/100 mM $NaNO_3$/1 mM $Ca(NO_3)_2$. Open symbols indicate the forces measured during the approach of the protein layers. Filled symbols show the force profile measured during separation of the protein monolayers, and the outward-directed arrow shows the position at which the adhesive bonds yield and the surfaces jump apart. *b* illustrates the proposed relative protein alignments with the corresponding domain numbers at the different stages of the force curve.

disks were rinsed gently with a syringe to remove nonspecifically bound protein and then mounted in the apparatus.

In control measurements of forces between cadherin monolayers and bare 25 mol% DSIDA membranes, the cadherin was first dialyzed against a calcium-free buffer for 12 hr at 4°C to remove any antiparallel protein complexes that might be present. The dialyzed protein was then bound to 50 mol% DSIDA monolayers, and calcium was added to the bathing solution. Separate experiments showed the protein activity was recovered after the readdition of calcium.

The dependence of the amount of adsorbed cadherin as a function of the DSIDA mol fraction in the outer bilayer leaflet was quantified with a home-built surface plasmon resonance instrument based on the Kretschmann configuration (16, 17). For the plasmon resonance measurements, the DSIDA monolayers were deposited on self-assembled hexadecanethiol monolayers on thin gold films, which were evaporated onto glass slides. The coated glass slides were mounted in a parallel plate flow cell, and the amount of cadherin adsorbed was determined from the net change in the plasmon resonance angle after cadherin binding. The bulk cadherin concentration in the bathing solution was the same as used to prepare the surface force apparatus (SFA) samples. The instrumental setup and data analysis methodology have been described elsewhere (17).

Force Measurements. Forces between protein monolayers were measured with a Mark III SFA (SurForce, Santa Barbara, CA). With this instrument, one quantifies directly the molecular forces between monomolecular films as a function of the film separation distance. The materials of interest are confined to the surfaces of two crossed-cylindrical lenses. Positioning controls vary the spacing between the samples, and the deflection in a spring supporting the lower sample gives the force between them. The force resolution is ±1 nN. With the optical interferometric technique of the SFA, one can determine the intersurface spacing *in situ* with a resolution of ±0.1 nm (12).

Results

Definition of the Intersurface Separation Distance, *D*. In the measured force-distance curves between identical cadherin monolayers, the distance *D* refers to the separation between the dehydrated surfaces of the bilayers that support the proteins. In control measurements in which we quantified the forces between a cadherin monolayer and a bare DSIDA/DTPC membrane, *D* is the distance between the bare membrane surface and the surface of the bilayer supporting cadherin.

The bilayer separation *D* was determined in two ways. In the first approach, we measured *in situ* the change in the thickness T_1 of the organic layers between the DPPE monolayers after the deposition of the DSIDA/DTPC monolayers and the subsequent adsorption of cadherin (Fig. 1). Thus, $D = T_1 - 2(T_{DSIDA})$, where T_{DSIDA} is the thickness of the DSIDA monolayer. In the second method, the total thickness of all organic films between the mica substrates T_2 was determined from the change in the distance of closest intersurface approach after stripping all organic layers from the mica substrates (Fig. 1). The latter is done by draining the liquid from the apparatus and then burning off the organic layers by UV irradiation (15, 18). In this case, $D = T_2 - 2(T_{DSIDA} + T_{DPPE})$. Here T_{DPPE} is the thickness of the DPPE monolayer. Note that $T_2 = T_1 + 2T_{DPPE}$. Importantly, the 2.5-nm thickness of the DPPE and the 3.2-nm thickness of the DSIDA monolayers were determined in independent measurements and have also been reported elsewhere (19, 20). Because the bilayer thicknesses are known and either T_1 or T_2 are measured directly in each experiment, $D = 0$ is determined unambiguously. This is an important distinction from other force probes where the distances are generally relative to some arbitrary reference position. This is of particular importance for determining (*i*) the dimensions of the cadherin monolayers and (*ii*) the locations of the adhesive minima between the proteins.

With the thus determined bilayer separation distances, the thicknesses of the cadherin monolayers are also determined from the bilayer separation *D* at the onset of steric repulsion either between opposing dilute cadherin monolayers or between a cadherin monolayer and a bare DSIDA membrane. For example, the measured onset of steric repulsion between cadherin and a bare lipid bilayer occurred at 23 nm (mica–mica separation T_2 = 34.5 nm). This directly measured unadjusted value is in good agreement with the estimated 22-nm length of the ectodomain on the basis of the crystallographically determined dimensions of EC1–2 and electron micrographs of the full-length extracellular fragment (9, 21).

Force Measurements. Fig. 2 shows the force curve measured during both the approach and the separation of cadherin mono-

BIOPHYSICS

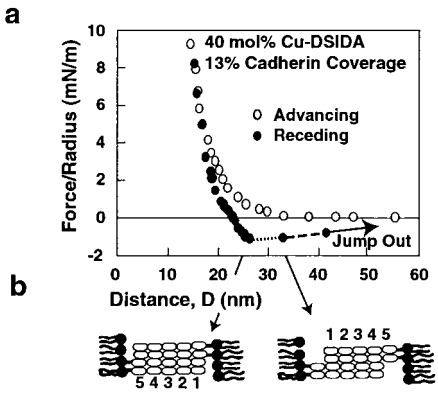

Fig. 3. (*a*) Normalized force vs. the distance between membranes displaying cadherin at 13% surface coverage. The supporting lipid monolayers comprised 40 mol% Cu-DSIDA and 60 mol% DTPC. The initial slow detachment from 26 nm is indicated by the dotted line. The dashed line shows the region of intermediate detachment velocity (>0.5 nm/s). The outward directed arrow at 44 nm shows the final rupture of the protein–protein junction. The proposed protein orientations are shown in *b*.

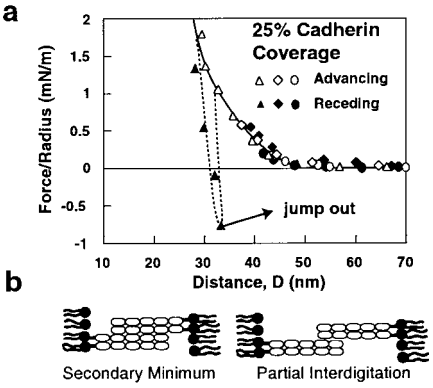

Fig. 4. (*a*) "Partial interdigitation" measurements obtained with cadherin monolayers at 25% surface coverage. Successive measurements correspond with successively decreasing intermembrane separations *D*. The circles indicate the forces measured during the approach ( ) and retraction ( ) of the protein films for the closest intermembrane distance of 40 nm. The diamonds indicate a successive measurement in which the distance of closest membrane approach was 37 nm, and the open and filled triangles indicate advancing and receding measurements, respectively, to and from 29 nm. The solid arrow shows the jump-out from the adhesive minimum at 32 nm. (*b*) The proposed protein alignments at partial protein interdigitation.

layers on 25 mol% DSIDA bilayers. On these membranes, the cadherin surface density, determined by surface plasmon resonance, was 70 nm^2/cadherin. This is 7% of a close-packed cadherin monolayer, assuming an end-on orientation. Between these dilute protein films, the advancing profiles exhibited no force at $D > 25$ nm. Because the linear dimension of the full-length extracellular domain is 22 ± 1 nm (9, 21, 22), and the length of the DSIDA linker is *ca.* 1 nm, the proteins should interdigitate completely at $D < 25 \pm 1$ nm (9, 21, 22). We therefore attribute the repulsive force at $D < 25$ nm to steric interactions between the proteins and the opposing bilayer surface.

Importantly, the minimum in the receding force curve at the intersurface separation of 26 ± 1 nm (Fig. 2*a*) indicates that the maximum adhesive force between cadherin involves fully interdigitated antiparallel extracellular domains (Fig. 2*b*). The adhesive force of -0.5 mN/m between these sparse protein monolayers is the force required to pull the proteins out of contact. At $D = 26 \pm 1$ nm, the interprotein bonds yielded, and the cadherin layers jumped out of contact. Furthermore, measurements between a cadherin monolayer and a bare 25 mol% DSIDA-Cu bilayer (data not shown) were reversible and exhibited no adhesion. This confirmed that the attraction between the two protein layers was caused by cadherin binding. There also was no adhesion in the absence of calcium (not shown). Calcium maintains the rigidity of the interdomain linkages and is required for cadherin activity (9, 21). Although we cannot specify which domains interact, these measurements show that the primary adhesive complex clearly involves completely interdigitated full-length ectodomains. By contrast, if homophilic cadherin adhesion involved the N-terminal domains alone (7), then the attractive minimum would lie at 40–45 nm.

To test whether the N-terminal domains adhere to each other, we reduced the interbilayer distance to between 33 nm and 44 nm and allowed the proteins to overlap partially before we again separated them (*cf.* Fig. 3). The absence of adhesion in these measurements showed that the N-terminal domains alone do not bind, or that the adhesive strength is below the ± 0.1 mN/m instrumental detection limit. These results do not rule out the involvement of the EC1 domains, for which there is some evidence (22, 23), but they do suggest that additional segments mediate binding and that the EC1 segment may interact with other domains.

We estimated the homophilic protein bond energy from the magnitude of the adhesive force and Johnson–Kendall–Roberts theory for the adhesion between deformable solids (24). The adhesion energy per area E is related to the adhesive force between the curved discs by $E = 2F/3\pi R$ where R is the geometric average radius of the disks. Normalizing the energy density by the surface coverage of cadherin (70 nm^2/protein) on the bilayers gives an average cadherin bond energy (assuming each protein forms a transmembrane bond) of 2 kT. This is substantially weaker than, for example, antibody–antigen interactions (15). Nevertheless, these proteins aggregate 1 μm beads, and cells expressing the full-length cadherin on their surfaces bind to monolayers of the CEC1–5, although less effectively than to the wild-type protein.

The most striking finding, however, is the unusual protein detachment behavior exhibited in the force profiles measured at higher protein densities (13% cadherin, 40 mol% Cu-DSIDA). In all previous force measurements of protein–ligand interactions, bond failure results in the abrupt snap of the molecules out of adhesive contact (14, 15, 25–32). By contrast, the cadherin unbinding profile (Fig. 3) occurred in three qualitatively distinct stages. As at the low-protein density, the bonds first yielded at 26 ± 1 nm. The adhesion of -0.9 ± 0.1 mN/m was about twice that measured at 7% cadherin coverage. However, the proteins did not jump abruptly out of contact. Instead they first moved apart slowly at 0.05 nm/s to 32 ± 1 nm. At $D > 32$ nm, the detachment velocity increased to >0.5 nm/s, and the proteins finally jumped out of contact from 44 ± 1 nm. We observed this behavior in five independent experiments with three separate protein preparations. The reproducibility both of the force curves and of the adhesion measured after initial detachment also showed that the lipid anchors did not pull out of the membrane (29). This indicates that rupture indeed occurred at the protein–protein contacts.

The advancing force curves were similar to those measured with more dilute protein layers. The slightly longer-range repulsive force measured at $D < 35$ nm is probably caused by the increased steric and osmotic force between the more crowded protein layers. At 25% cadherin coverage (*cf.* Fig. 4), the onset of the steric repulsion occurred still farther out at $D < 44$ nm. The range of the latter repulsion is consistent with interactions

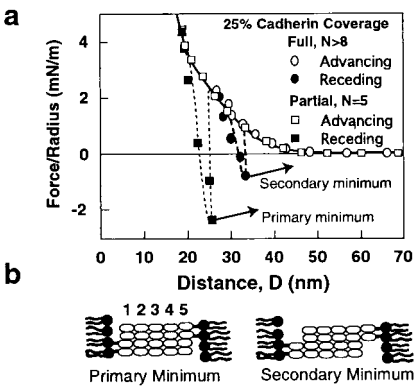

Fig. 5. (*a*) Composite force vs. distance curve showing the measured primary and secondary adhesive minima at 25% cadherin coverage. Open symbols indicate the advancing force curves and the filled circles show the receding force profiles. The arrows show the positions at which the bonds yielded. The sluggish unbinding regimes are not shown in this figure. (*b*) The proposed relative cadherin alignments at the positions of the two attractive minima.

between the protein ends and further supports the end-on orientation of the immobilized cadherin.

Two different mechanisms could generate the unusual detachment behavior: (*i*) viscous drag between adjacent proteins or (*ii*) additional adhesive minima impeding unbinding. To test the first possibility, we calculated the viscous drag acting on the protein cylinders as they are pulled out of a dense protein layer. By using the Derjaguin approximation (33), one can show that the lubrication force between end-anchored rods (34) bound to opposing crossed-cylinders at a particular surface density is given by

$$\frac{F}{R} = 2\pi\left[\frac{2\pi\mu V\rho}{Ln\left(\frac{r}{Y}\right)}\right]\frac{l^2}{2}, \qquad [1]$$

where μ is the bulk solvent viscosity, V is the axial velocity of the rods, ρ is the surface density of rods, r is the radius of the individual cadherin proteins, Y is the distance between the center of cadherin and the outer surface of an adjacent molecule in a dense interdigitated protein cluster, and l is the length of cadherin. With this macroscopic model and known protein dimensions (7, 9, 21), we calculated the viscous force between a 20% cadherin monolayer and a hypothetical densely populated surface in which nearest neighbors are within 0.5–0.6 nm of each other. Because the latter density is higher than achieved in actual experiments, we overestimated the lubrication force. Nevertheless, the calculated value was only 0.2 mN/m in the low-velocity regime (0.05 nm/s). This is an order of magnitude weaker than the adhesion of −2.5 mN/m measured at 25% cadherin coverage (*cf.* Fig. 5). Moreover, Eq. **1** predicts that the viscous drag, and hence the apparent interprotein attraction, would depend linearly on the velocity, V. By contrast, the strength of isolated bonds varies logarithmically with the detachment rate (35). Increasing the loading rate four-fold would increase the lubrication force correspondingly, but should alter the bond strength only by roughly 30%. In our studies, increasing the detachment rate roughly four-fold did not change the strength of adhesion. Friction cannot, therefore, account for the slowed unbinding and suggested that additional attractive protein interactions impeded the junction failure.

To investigate the second possible mechanism, we looked for additional adhesive minima by locating additional relative alignments at which the cadherin monolayers bind. One achieves this by controlling the degree of protein interdigitation by adjusting the interbilayer distance D. For example, at high-protein coverage (25%; Fig. 4), we reduced D to some value $D < 44$ nm and then separated the proteins. If no bonds form, then the forward (Fig. 4, open symbols) and corresponding reverse force curves (filled symbols) will be identical. Protein binding causes a negative deviation in the receding profile, and the protein monolayers jump out of contact when the bonds fail (Fig. 4, triangles). In this way, we measured a second attractive minimum at 32 ± 1 nm. The adhesion was −0.8 mN/m, which is *ca.* one-third the −2.5 mN/m measured between the fully interdigitated monolayers at 25% cadherin coverage. Sparse (7%) cadherin monolayers also adhered at 32 nm (not shown). Importantly, this secondary minimum is at the same protein separation where the detachment velocity increased from 0.05 nm/s to >0.5 nm/s. Moreover, the 6-nm distance between the primary and secondary minima is close to the 5-nm length of the individual cadherin domains (7, 9). Again, even between dense cadherin monolayers (25%), the lack of measured adhesion at $D > 32$ nm suggests that the N-terminal domains do not bind strongly (Fig. 4).

Discussion

The existence of multiple adhesive contacts between antiparallel cadherin ectodomains appears to explain the unusual detachment behavior observed at high cadherin coverage. Our interpretation is that protein slippage from the primary to the secondary minimum generates the sluggish unbinding trajectory (Figs. 3 and 5). The spacing between these minima is consistent with a ratchet model in which the domains adhere successively as the proteins are pulled apart. This process retards the abrupt rupture of the junction. We believe that the apparent absence of viscous unbinding at the low cadherin density is likely because the magnitude of the force in that case was insufficient to slow the protein detachment detectably. Similarly, although the unbinding velocity between the dense cadherin monolayers increased to >0.5 nm/s between 32 and 44 nm, the absence of measured adhesive minima in this distance range does not rule out their existence. Additional segment binding may be responsible for the sluggish detachment, but the attractive forces are below the detection limit of these measurements.

The detailed physical–chemical interactions responsible for adhesion between cadherin ectodomains have not been identified. To determine possible forces that may mediate binding, we estimated the van der Waals attraction between crossed cylinders coated with end-anchored rods comprising a string of five smooth beads with 1.25-nm radii. Depending on the values chosen for the interdomain distances, for example, our calculations indicate that the van der Waals force between aligned proteins could account for the measured adhesion. However, without additional biochemical and structural information, it is not possible to state definitively that this interaction alone governs cadherin binding. The calculations do suggest, however, that the van der Waals force, and hence cadherin adhesion, may increase with the number of contacts between antiparallel extracellular domains.

These force measurements demonstrate that the adhesion between C-cadherin extracellular domains involves the full-length extracellular region, and that there are at least two antiparallel adhesive alignments. Force measurements alone cannot, however, identify which domains mediate binding. Future studies with different cadherin mutants are therefore necessary for the identification of both the domains and the detailed protein contacts responsible for the observed adhesion. Force measurements with domain deletion mutants, for example, will quantify the contributions of the different domains to the total binding strength. Additionally, the align-

ment specificity of the binding contacts can be tested by genetically engineering changes in the relative spacing between the different cadherin domains. In addition to direct measurements of the proteins' adhesive function, biochemical analyses will be needed to establish the detailed molecular interactions responsible for recognition between cadherin extracellular domains.

The multiple discrete adhesive minima are not caused by the curvature of the supporting mica sheets (27) or random protein orientations. Simulations indicate that the curvature will not broaden the potential, and that discrete minima in the protein–protein interaction will generate discrete minima in the intersurface potential (36). The rigidity of the cadherin extracellular domain, inferred from the steep protein–membrane repulsion, insures that the protein–protein potential will not be distributed over a large distance (27) and that the profile will therefore exhibit distinct adhesive minima. By contrast, the attachment of biotin to a flexible structureless polymer chain thus broadened the streptavidin–biotin interaction potential (27). Finally, random protein orientations also would not generate the distinct minima reported here.

In summary, the unusual cadherin detachment behavior we report suggests the evolution of a special mechanism for resisting the abrupt failure of cell–cell junctions. The adhesion between interdigitated antiparallel extracellular domains allows for multiple cadherin binding interactions. These in turn may generate a built-in "catch mechanism," which further impedes abrupt junction failure should the primary cadherin contacts rupture. The multiple-stage unbinding mechanism reported here has, to our knowledge, not been observed previously. Although other proteins exhibit abrupt bond failure, and hence more brittle contacts, the multiple-stage rupture displayed by cadherin may impart greater flexibility to the intercellular junctions.

This work was supported by National Science Foundation (NSF) BES 9503045CAR (D.E.L.) and by National Institutes of Health GM 52717 (B.M.G.) and the Cancer Center NCI-P30-CA-08748 (B.M.G.). The force apparatus was purchased with funds from NSF grant BES 9622761 (D.E.L.). We thank Frances Arnold for the generous gift of the DSIDA lipid.

1. Takeichi, M. (1995) *Curr. Opin. Cell Biol.* **7,** 619–627.
2. Yap, A. S., Brieher, W. M. & Gumbiner, B. M. (1997) *Annu. Rev. Cell. Dev. Biol.* **13,** 119–146.
3. Gumbiner, B. M. (1996) *Cell* **84,** 345–357.
4. Takeichi, M. (1991) *Science* **251,** 1451–1455.
5. Brieher, W. M., Yap, A. S. & Gumbiner, B. M. (1996) *J. Cell Biol.* **135,** 487–496.
6. Yap, A. S., Niessen, C. M. & Gumbiner, B. M. (1998) *J. Cell. Biol.* **141,** 779–789.
7. Shapiro, L., Fannon, A. M., Kwong, P. D., Thompson, A., Lehmann, M. G., Grübel, G., Legrand, J.-F., Als-Nielsen, J., Colman, D. R. & Hendrickson, W. A. (1995) *Nature (London)* **374,** 327–337.
8. Tamura, K., Shan, W.-S., Hendrickson, W. A., Colman, D. R. & Shapiro, L. (1998) *Neuron* **20,** 1153–1163.
9. Nagar, B., Overduin, M., Ikura, Mitsuhiko & Rini, J. M. (1995) *Nature (London)* **380,** 360–364.
10. Weis, W. I. (1995) *Structure (London)* **3,** 425–427.
11. Leckband, D. (1995) *Nature (London)* **376,** 617–618.
12. Israelachvili, J. (1992) *Surf. Sci. Rep.* **14,** 110–159.
13. Ng, K., Pack, D., Sasaki, D. Y. & Arnold, F. H. (1994) *Langmuir* **11,** 4048–4055.
14. Leckband, D., Schmitt, F.-J., Israelachvili, J. & Knoll, W. (1994) *Biochemistry* **33,** 4611–4624.
15. Leckband, D. E., Kuhl, T. L., Wang, H. K., Müller, W. & Ringsdorf, H. (1995) *Biochemistry* **34,** 11467–11478.
16. Kretschmann, E. & Raether, H. (1968) *Z. Naturforsch. A Phys. Phys. Chem. Kosmophys.* **23,** 2135–2136.
17. Yeung, C., Purves, T., Kloss, A. A., Kuhl, T. L., Sligar, S. & Leckband, D. (1999) *Langmuir,* in press.
18. Leckband, D. E., Helm, C. A. & Israelachvili, J. (1993) *Biochemistry* **32,** 1127–1140.
19. Marra, J. & Israelachvili, J. (1985) *Biochemistry* **24,** 4608–4618.
20. Wu, Z.-W., Calvert, T. L. & Leckband, D. (1997) *Biochemistry* **37,** 1540–1550.
21. Pokutta, S., Herrenknecht, K., Kemler, R. & Engel, J. (1994) *Eur. J. Biochem.* **223,** 1019–1026.
22. Tonschy, A., Fauser, C., Landwehr, R. & Engel, J. (1996) *EMBO J.* **15,** 3507–3514.
23. Nose, A., Tsuji, K. & Takeichi, M. (1990) *Cell* **61,** 147–155.
24. Johnson, K. L., Kendall, K. & Roberts, A. D. (1971) *Proc. R. Soc. London A* **324,** 301–313.
25. Wong, S., Joselevich, E., Woolley, A. T., Cheung, C. L. & Lieber, C. M. (1998) *Nature (London)* **394,** 52–55.
26. Yip, C. M., Yip, C. C. & Ward, M. D. (1998) *Biochemistry* **37,** 5439–5449.
27. Wong, J. Y., Kuhl, T. L., Israelachvili, J. N., Mullah, N. & Zalipsky, S. (1997) *Science* **275,** 820–822.
28. Moy, V. T., Florin, E.-L. & Gaub, H. E. (1994) *Science* **266,** 257–259.
29. Leckband, D., Müller, W., Schmitt, F.-J. & Ringsdorf, H. (1995) *Biophys. J.* **69,** 1162–1169.
30. Florin, E.-L., Moy, V. T. & Gaub, H. E. (1994) *Science* **264,** 415–417.
31. Chilkoti, A., Boland, T., Ratner, B. D. & Stayton, P. S. (1995) *Biophys. J.* **69,** 2125–2130.
32. Lee, G. U., Kidwell, D. A. & Colton, R. J. (1994) *Langmuir* **10,** 354–357.
33. Israelachvili, J. (1992) *Intermolecular and Surface Forces* (Academic, New York).
34. Bird, R., Stewart, W. & Lightfoot, E. (1960) *Transport Phenomena* (Wiley, New York), Chapter 2.
35. Evans, E. & Ritchie, K. (1997) *Biophys. J.* **72,** 1541–1555.
36. Vijayendran, R., Hammer, D. & Leckband, D. (1998) *J. Chem. Phys.* **108,** 1162–1169.